JOURNAL OF THEORETICAL AND APPLIED MECHANICS
49, 3, pp. 879-903, Warsaw 2011

SIMULATION OF WAVE PROPAGATION IN DAMPED COMPOSITE STRUCTURES WITH PIEZOELECTRIC COUPLING

Rolf T. Schulte
Claus-Peter Fritzen

University of Siegen, Institute of Mechanics and Automatic Control – Mechatronics, Siegen, Germany; e-mail: fritzen@imr.mb.uni-siegen.de

This paper presents an efficient and accurate simulation approach to shorten time and cost of the necessary pre-tests in the design process of structural health monitoring (SHM) systems. The simulation is performed using the time domain spectral element method, which leads to an optimally concentrated mass matrix and results in a crucial reduction of complexity of the time integration algorithm. The theoretical background of the method and a spectral element for flat shells are presented. New approaches to incorporate the anisotropic material damping and an efficient coupling of piezoelectric elements within the spectral element framework are developed.
Some numerical calculations are performed showing both the accuracy of this methodology, by comparing to experimental values, and the applicability to more complex structures like stiffened curved panels.

Key words: spectral element method, composites, anisotropic attenuation

1. Introduction

During the last decades, many structural health monitoring (SHM) approaches based on activating and sensing elastic waves using piezoelectric patches have been developed (Balageas *et al.*, 2006; Giurgiutiu, 2007). The majority of these systems have shown their capabilities in the laboratory environment, and their technology readiness level (TRL) is in the range of two to five, compare Mankis (1995). So far, there are few examples of the transfer to more complex real world structures. The reason for this can be found in many obstacles

arising from different sectors: complexity of the technology, manufacturing, certification, regulation authorities and some more.

This paper concentrates on the first of these points, the complexity of the technology itself. Many wave propagation phenomena and especially the interactions with different kinds of damage are difficult to understand. This is particularly true with regard to received sensor data because of the presence of different wave modes that often cannot be distinguished. However, only a profound comprehension of wave propagation leads to the ability to configure optimized SHM systems for a desired application. The system performance strongly depends on an adequate choice of parameters like excitation signals, damage evaluation algorithms, actuator/sensor types and actuator/sensor distribution. For successful monitoring of complex real world structures, the influence of all these parameters has to be studied in detail. For this reason there is a strong interest in accurate simulation and visualisation tools to give insight into the details of the wave motion. Precise and efficient numerical modelling techniques can help to cut time and cost of the parameter optimization process, and thereby can assist the challenging step to real world structures and higher TRLs.

Generally, for the modelling of wave propagation phenomena a variety of methods can be utilised. Well-established are the finite difference method (FDM) (Graves, 1996), the pseudospectral method (PSM) (Fornberg, 1987; Ku *et al.*, 1987), the finite element method (FEM) (Moser *et al.*, 1999; Zienkiewicz *et al.*, 2005) and the boundary element method (BEM) (Beskos, 1997; Cho and Rose, 1996). Because of the high frequency signals, which are required to detect small damage, a very dense finite element mesh is necessary for accurate simulation of wave propagation and possible wave scattering at defects. For that reason, the conventional finite element simulation becomes computationally very inefficient. Finite difference methods suffer from numerical dispersion and difficulties arise when implementing boundary conditions (Graves, 1996). Other approaches use mass-spring-lattice models (MSLM), see e.g. Yim and Sohn (2000). Developments in this field include the so called local interaction simulation approach (LISA), in which wave propagation is simulated without using finite difference equations, but directly from physical phenomena and properties (Delsanto *et al.*, 1997).

A quite different methodology is the utilisation of so called spectral elements. Using this terminology, it is important to clearly distinguish between two different techniques known under the same term. The Fourier transformation based spectral elements, see Doyle (1997), start from exact solutions of the partial differential equations in the frequency domain. The excitation signals

are transferred to the frequency domain using Fast Fourier Transformation (FFT) and after solving the inverse FFT is used to calculate the response in the time domain. This technique shows very good results for one-dimensional structures (beams, rods) but difficulties arise in handling more complex geometries, because exact solutions of the problem are often not available.

A more promising method for complex structures is the time domain spectral element method (SEM) that was first proposed by Patera (1984). It combines the accuracy of the global pseudospectral method with the flexibility of the FEM. However, the spectral element method is not widespread in the context of wave propagation in thin-walled structures. In Kudela *et al.*(2007) and Kudela and Ostachowicz (2009) spectral elements are used to simulate transverse wave propagation in undamped composite plates. In Ostachowicz(2008) different elements (rods, beams, plates) based on the spectral element method including damage models are derived. In Peng *et al.* (2009) waves in planar shells are calculated by means of spectral volume elements. The SEM is used in recent publications to investigate the wave propagation and interaction with damages in complex structures like a welded L-joint (Rucka, 2010) or a half-pipe structure (Ostachowicz and Kudela, 2010).

In this paper, the formulation of a flat shell spectral element is presented, including consideration of material damping. The construction of mass-, stiffness- and damping matrices, and the time integration algorithm are presented briefly. A model of the electromechanical coupling of piezoelectric actuators and sensors is adapted and integrated into the spectral element framework. By construction, this leads to an efficient tool to simulate wave propagation phenomena in thin-walled structures. An example of propagating waves in a unidirectional composite plate is presented including the comparison of simulation results with measured data. Moreover, a model of a curved panel with stiffeners is analysed to demonstrate the applicability to more complex-shaped geometries. The simulation results of the presented model can be used to develop advanced signal processing strategies and to perform detailed parameter studies.

2. Nodal base and shape functions in the spectral element method

For the numerical treatment of high-frequency wave propagation one important aspect to be kept in mind is the necessity of a dense mesh-grid to account for the short wavelength. This requires to consider the interpolation properties

of the used element type to be able to capture the wave motion with as few degrees of freedom as possible. Theoretical analysis shows that the highest interpolation accuracy is achieved by distributing the interior nodes of an element corresponding to the roots of certain orthogonal polynomials, namely Chebyshev or Lobatto polynomials (Pozrikidis, 2005). In contrast to the Chebyshev polynomials, the $N+1$ nodes of the Lobatto nodal base, the roots of equation (2.1)

$$(1-\xi^2)Lo_{N-1}(\xi) \tag{2.1}$$

in conjunction with Lagrange interpolation polynomials leads by construction to an optimally concentrated mass matrix as will be seen subsequently. $Lo_{N-1}(\xi)$ denotes the Lobatto polynomial of $(N-1)$-th order. The Lagrange interpolation polynomials fulfil the discrete orthogonality $\psi_i(\xi_j)=\delta_{ij}$ where δ_{ij} denotes the Kronecker delta. In Fig. 1 these interpolation polynomials – also called shape functions – are depicted within the one-dimensional reference domain for a nodal base of 7 Gauss-Lobatto-Legendre (GLL) nodes. The discrete orthogonality can be clearly seen as each polynomial is exactly one at its corresponding GLL node and zero at all other nodes.

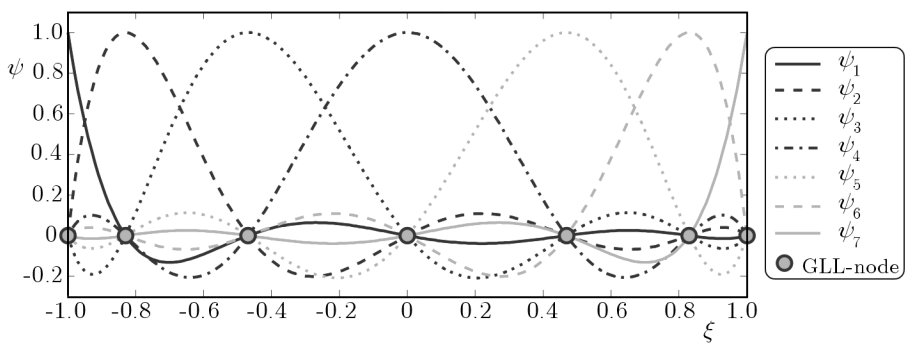

Fig. 1. Lagrange interpolation polynomials on the reference interval $[-1,1]$ through 7 Gauss-Lobatto-Legendre (GLL) points

Moreover, the excellent interpolation properties of this kind of elements can be seen in Fig. 1, because the shape functions vary smoothly between approximately -0.2 and 1 and any kind of Runge oscillations, that occur at the ends of a higher order element with evenly spaced nodes when the polynomial order is raised, are totally suppressed.

For the extension to two-dimensional elements, as the flat shell elements presented within this paper, quadrilateral elements based on a tensorial product of the one-dimensional constituents should be favoured over triangular elements. The tensorial product guarantees that the discrete orthogonality

also holds for the two-dimensional shape functions. If triangular elements have to be used, Fekete points should be used as the nodal base (Komatitsch *et al.*, 2001; Pozrikidis, 2005), but with respect to accuracy and numerical stability quadrangles are preferable, as it is stated in Komatitsch *et al.* (2001). According to Seriani, only about 5 to 6 nodes (exact value depends on the degree of the interpolation polynomial) per shortest wavelength are necessary to correctly simulate the wave propagation behaviour in contrast to 15-30 which are needed using lower order finite elements (Seriani and Priolo, 1994).

3. Flat shell spectral element for composite material

The flat shell spectral element presented here is based on the first order shear deformation theory (FSDT) for plates that was developed by Mindlin. The three independent displacements $\widetilde{u}$, $\widetilde{v}$ and $\widetilde{w}$ are expressed using a displacement field of the form

$$\begin{aligned}
\widetilde{u}(x,y,z,t) &= u(x,y,t) + \frac{\partial z_0}{\partial x} w(x,y,z,t) + z\theta_y(x,y,t) \\
\widetilde{v}(x,y,z,t) &= v(x,y,t) + \frac{\partial z_0}{\partial y} w(x,y,z,t) - z\theta_x(x,y,t) \\
\widetilde{w}(x,y,z,t) &= w(x,y,z,t)
\end{aligned} \tag{3.1}$$

where $(u, v, w, \theta_x, \theta_y)$ are unknown functions to be determined. u, v and w are the displacement of the plane $z = 0$, θ_x and θ_y denote right-hand-rule rotations, see Fig. 2.

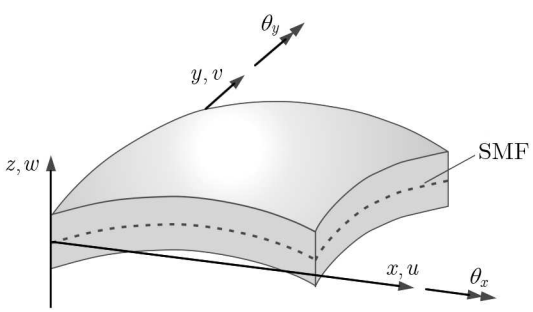

Fig. 2. Kinematic parameters used for the description of a flat shell element, the dashed line is the midface of the shell

A rotational dof θ_z about the local z-axis is not used within the kinematic description. This inhibits arbitrary transformations of the elements in space between local and global coordinates, because general transformations in

space account for 6 dofs. In principle, it is possible to use an in-plane formulation with explicit θ_z-dof but this would complicate the problem unnecessarily. Instead, an artificial θ_z-dof that is not used within the kinematic formulation, can be introduced. To regularise the resulting system of equations, small artificial values for the stiffness and mass of this dof are defined following Bathe (1986). The terms $(\partial z_0/\partial x)w(x,y,z,t)$ and $(\partial z_0/\partial y)w(x,y,z,t)$ take into account the curvature of the shell in form of a pre-deformation, see Wagner (1985). For planar shells, these terms are dropped.

The displacement field on the element level can be approximated in the following form

$$\begin{bmatrix} w(\xi,\eta) \\ \theta_x(\xi,\eta) \\ \theta_y(\xi,\eta) \\ u(\xi,\eta) \\ v(\xi,\eta) \end{bmatrix} = \sum_{i=1}^{N+1}\sum_{j=1}^{N+1} \Psi_{ij}(\xi,\eta)\boldsymbol{q}_{ij}^{(e)} = \sum_{i=1}^{N+1}\sum_{j=1}^{N+1} \psi_i(\xi)\psi_j(\eta) \begin{bmatrix} \widehat{w}(\xi_i,\eta_j) \\ \widehat{\theta}_x(\xi_i,\eta_j) \\ \widehat{\theta}_y(\xi_i,\eta_j) \\ \widehat{u}(\xi_i,\eta_j) \\ \widehat{v}(\xi_i,\eta_j) \end{bmatrix} \tag{3.2}$$

where ξ and η denote the local element coordinates, Ψ is a two-dimensional shape function and ψ_i is the i-th one-dimensional shape function defined above. $\boldsymbol{q}^{(e)}$ represents the vector of nodal variables and the hat indicates nodal degrees of freedom that are the unknowns of the resulting system of equations. Examples of the GLL nodal distribution within the two-dimensional reference element are depicted in Fig. 3 for a 25-node and a 81-node element. Raising the degree of the interpolation polynomial – that is increasing the number of nodes per element – leads to clustering of nodes at the element corners. The implication of this effect is discussed subsequently.

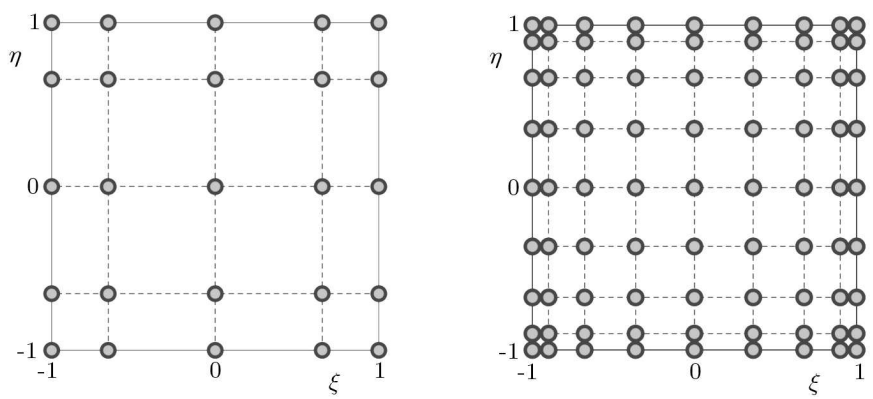

Fig. 3. Nodal distribution within the reference element for 5 GLL nodes (left) and 9 GLL nodes (right) per element edge

Some examples of the two-dimensional shape functions Ψ on a grid using 25 element nodes are given in Fig. 4.

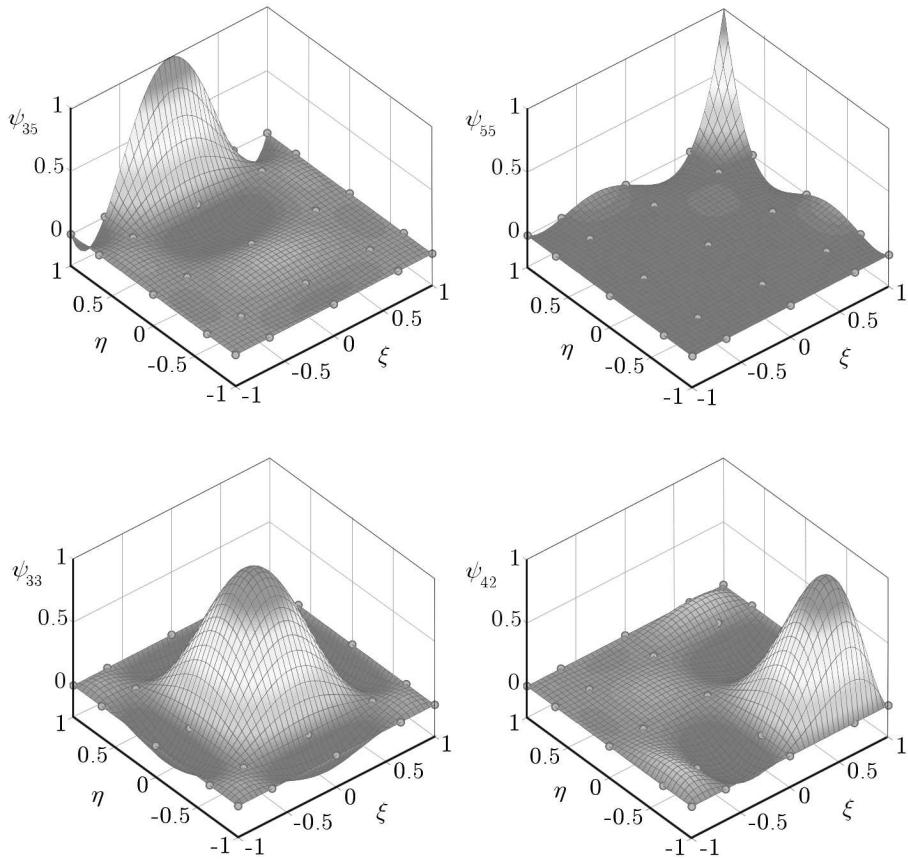

Fig. 4. Examples of shape functions Ψ_{ij} of a spectral-shellelement with 5 GLL-nodes per element edge

The derivation of the variational equation and the weak form follows the standard FE procedures, see e.g. Hughes (1987). The element matrices are calculated using the Gauss-Lobatto integration rule. For the stiffness matrix this leads to

$$\begin{aligned}\mathbf{K}^{(e)} &= \iint_{\Omega^e} [\mathbf{B}(x,y)]^\top \mathbf{D}\mathbf{B}(x,y)\det(\mathbf{J})\, d\Omega \\ &\approx \sum_{i=1}^{N+1}\sum_{j=1}^{N+1} \overline{w}_i \overline{w}_j [\mathbf{B}(x_{ij},y_{ij})]^\top \mathbf{D}\mathbf{B}(x_{ij},y_{ij})\det(\mathbf{J})\end{aligned} \tag{3.3}$$

where $\overline{w}$ are quadrature weights and $\mathbf{D}$ is the material stiffness matrix that is defined as

$$\mathbf{D} = \begin{bmatrix} D_{11} & D_{12} & D_{16} & 0 & 0 & B_{11} & B_{12} & B_{16} \\ D_{12} & D_{22} & D_{26} & 0 & 0 & B_{12} & B_{22} & B_{26} \\ D_{16} & D_{26} & D_{66} & 0 & 0 & B_{16} & B_{26} & B_{66} \\ 0 & 0 & 0 & \kappa A_{55} & \kappa A_{45} & 0 & 0 & 0 \\ 0 & 0 & 0 & \kappa A_{45} & \kappa A_{44} & 0 & 0 & 0 \\ B_{11} & B_{12} & B_{16} & 0 & 0 & A_{11} & A_{12} & A_{16} \\ B_{12} & B_{22} & B_{26} & 0 & 0 & A_{12} & A_{22} & A_{26} \\ B_{16} & B_{26} & B_{66} & 0 & 0 & A_{16} & A_{26} & A_{66} \end{bmatrix} \tag{3.4}$$

where κ is a shear correction factor. The mass matrix can be calculated as

$$\begin{aligned} \mathbf{M}^{(e)} &= \iint_{\Omega^e} [\mathbf{\Psi}(x,y)]^\top \mathbf{H} \mathbf{\Psi}(x,y) \det(\mathbf{J}) \, d\Omega \\ &\approx \sum_{i=1}^{N+1} \sum_{j=1}^{N+1} \overline{w}_i \overline{w}_j [\mathbf{\Psi}(x_{ij}, y_{ij})]^\top \mathbf{H} \mathbf{\Psi}(x_{ij}, y_{ij}) \det(\mathbf{J}) \end{aligned} \tag{3.5}$$

where $\mathbf{H}$ is given in the following equation

$$\mathbf{H} = \begin{bmatrix} I_0 & 0 & 0 & 0 & 0 \\ 0 & I_2 & 0 & 0 & -I_1 \\ 0 & 0 & I_2 & I_1 & 0 \\ 0 & 0 & I_1 & I_0 & 0 \\ 0 & -I_1 & 0 & 0 & I_0 \end{bmatrix} \tag{3.6}$$

The mass moments of inertia I_i are given according to

$$\begin{bmatrix} I_0 \\ I_1 \\ I_2 \end{bmatrix} = \int_{h^e} \begin{bmatrix} 1 \\ z \\ z^2 \end{bmatrix} \rho(z) \, dz \tag{3.7}$$

where ρ is the material density.

The mass matrix is optimally concentrated by construction because of the aforementioned discrete orthogonality of the shape functions. For a density distribution that is symmetric towards the midplane of the shell, the terms I_1 in the matrix $\mathbf{H}$ vanish. Therefore, a completely diagonal mass matrix results in that case.

Both $\mathbf{K}^e$ and $\mathbf{M}^e$ can be assembled in the same manner as it is done with the conventional finite elements to form global stiffness and mass matrices $\mathbf{K}$ and $\mathbf{M}$. The spectral elements naturally lead to free-free boundaries, other boundary conditions can be implemented as for low-order finite elements.

4. Incorporation of material damping

For a realistic simulation model of a composite material, the influence of attenuation has to be considered. While in other papers this point is neglected for simplicity (e.g. Kudela and Ostachowicz, 2009) the incorporation of damping into the spectral element framework for composite shells is an important aspect of this contribution.

The viscous damping model that is often applied in finite element analysis of dynamics of structures, assumes the equation of motion in the following form

$$\mathbf{M}\ddot{\boldsymbol{q}} + \mathbf{C}\dot{\boldsymbol{q}} + \mathbf{K}\boldsymbol{q} = \mathbf{F}(t) \tag{4.1}$$

The damping matrix $\mathbf{C}$ is usually assumed proportional to the mass and stiffness matrix

$$\mathbf{C} = \alpha\mathbf{M} + \beta\mathbf{K} \tag{4.2}$$

where the scalar coefficients α and β are determined from experimental measurements. Besides these models, some other approaches are used, especially the application of fractional derivatives seems promising (Bagley and Torvik, 1985).

Within this contribution, viscous damping is assumed leading to an equation of motion in form of Eq. (4.1). Indeed, in contrast to Eq. (4.2), the damping matrix is assembled in a different manner. As can be noticed from experiments on composite plates, the damping behaviour often shows an inverse proportionality to the in-plane stiffness. For that reason, the second term in Eq. (4.2), the linear coupling with the stiffness matrix, is completely dropped. However, the proportionality to the mass matrix alone is not able to take into account the direction-depending attenuation behaviour.

Instead, the following material damping matrix is introduced for each layer

$$\mathbf{C}_{mat}^{(k)} = \begin{bmatrix} \frac{1}{2}(C_{\theta f}^{(k)} + C_{\theta m}^{(k)}) & 0 & 0 & 0 & 0 \\ 0 & C_{\theta m}^{(k)} & 0 & 0 & 0 \\ 0 & 0 & C_{\theta f}^{(k)} & 0 & 0 \\ 0 & 0 & 0 & C_{f}^{(k)} & 0 \\ 0 & 0 & 0 & 0 & C_{m}^{(k)} \end{bmatrix} \tag{4.3}$$

providing different coefficients for the different degrees of freedom. Index f denotes the fibre direction, index m the transverse direction. This matrix can be formulated for each of the material layers separately in the material coordinate system, where the first axis is parallel to the fibre direction, see Fig. 5.

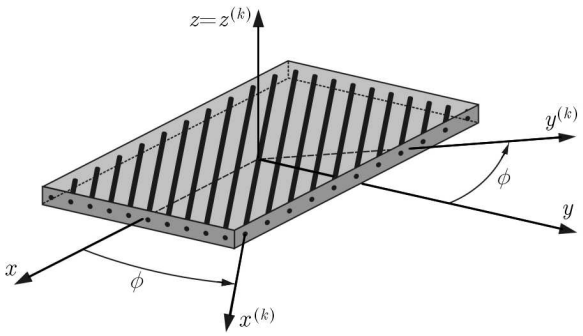

Fig. 5. Laminate coordinate system (x, y, z) and k-th layer with its material coordinate system $(x^{(k)}, y^{(k)}, z^{(k)})$

The material damping matrices from Eq. (4.3) can be transformed into the laminate coordinate system by using

$$\overline{\mathbf{C}}_{mat}^{(k)} = \mathbf{T}_c(-\phi^{(k)})\mathbf{C}_{mat}^{(k)}\mathbf{T}_c^{\top}(-\phi^{(k)}) \tag{4.4}$$

where the matrix $\mathbf{T}_c$ is an appropriate rotation matrix.

Finally, the material damping matrix for the laminate

$$\mathbf{C}_{mat} = \int_{h^e} \overline{\mathbf{C}}_{mat}\, dz = \sum_{k=1}^{L} \int_{z_k}^{z_{k+1}} \overline{\mathbf{C}}_{mat}^{(k)}\, dz \tag{4.5}$$

and the element damping matrix can be constructed

$$\begin{aligned} \mathbf{C}^{(e)} &= \iint_{\Omega^e} [\mathbf{\Psi}(x_{ij}, y_{ij})]^{\top} \mathbf{C}_{mat} \mathbf{\Psi}(x_{ij}, y_{ij}) \det(\mathbf{J})\, d\Omega \\ &\approx \sum_{i=1}^{N+1} \sum_{j=1}^{N+1} \overline{w}_i \overline{w}_j [\mathbf{\Psi}(x_{ij}, y_{ij})]^{\top} \mathbf{C}_{mat} \mathbf{\Psi}(x_{ij}, y_{ij}) \det(\mathbf{J}) \end{aligned} \tag{4.6}$$

If this approach is used on the element level, different attenuation coefficients can be used for the fibre direction and the transverse direction. With this methodology, two important properties are achieved: on the one hand, the direction-dependent attenuation behaviour can be realised and the damping coefficients of in-plane and out-of-plane waves can be chosen separately. On the other hand, the resulting damping matrix is diagonal. This property preserves the opportunity to make use of a rapid time integration scheme, which will be explained during the next section.

5. Time integration of the global system

The equation of motion of the global system (4.1) can be discretised in time using either implicit or explicit time integration schemes. To fully utilise the advantage of the diagonal mass and damping matrices, the explicit central difference scheme is used here. The main assumption of the central difference scheme is an acceleration of the form

$$\ddot{\boldsymbol{q}}^t = \frac{1}{\Delta t^2}(\boldsymbol{q}^{t-\Delta t} - 2\boldsymbol{q}^t + \boldsymbol{q}^{t+\Delta t}) \tag{5.1}$$

The velocity can be assumed as

$$\dot{\boldsymbol{q}}^t = \frac{1}{2\Delta t}(-\boldsymbol{q}^{t-\Delta t} + \boldsymbol{q}^{t+\Delta t}) \tag{5.2}$$

Inserting (5.1) and (5.2) into the system of ordinary differential equations (4.1) at the time instant t results in

$$\Big(\frac{1}{\Delta t^2}\mathbf{M} + \frac{1}{2\Delta t}\mathbf{C}\Big)\boldsymbol{q}^{t+\Delta t} = \mathbf{F}^t - \Big(\mathbf{K} - \frac{2}{\Delta t^2}\mathbf{M}\Big)\boldsymbol{q}^t - \Big(\frac{1}{\Delta t^2}\mathbf{M} - \frac{1}{2\Delta t}\mathbf{C}\Big)\boldsymbol{q}^{t-\Delta t} \tag{5.3}$$

that can be solved for $\boldsymbol{q}^{t+\Delta t}$. The solution of Eq. (5.3) can be performed very efficiently if matrix inversions can be avoided, which is the case if $\mathbf{M}$ and $\mathbf{C}$ are diagonal matrices. This methodology allows rapid calculation of the time dependent solution of the system. If these matrices are not diagonal, the term in brackets on the left hand side of Eq. (5.3) has to be decomposed, which increases the computational cost drastically. If instead of the GLL interpolation, Chebyshev polynomials are used, the mass matrix is no longer diagonal. In this case, either an iterative time-stepping algorithm could be used (Seriani, 2004) or the mass- and damping matrices can be diagonalised by row-summing the contributions on the diagonal (Dauksher and Emert, 2000).

The drawback of this scheme is the difficulty to set the timestep Δt that has to be appropriately small to reach stability of the solution. It is very difficult to derive a generally applicable formula to compute this timestep for wave propagation problems. It depends on many parameters like the maximal velocity of the travelling wave v_{max}, the excitation frequency, the distortion of elements and minimum distance of mesh-nodes Δx_{min}. The optimal length of the time increment Δt has to be adjusted to the particular problem of interest. It can be estimated by using the Courant-Friedrichs-Levy condition

$$\Delta t_{max} = CFL\frac{\Delta x_{min}}{v_{max}} \tag{5.4}$$

CFL is the Courant-number that is close to 0.85 for the one-dimensional case, but can only be estimated for more complex situations. The positive aspect of this particular problem is the fact that a numerical error resulting from a too large timestep Δt makes the solution grow very fast to infinity. This behaviour enables the user to distinguish easily between the correct results and numerically distorted results by the too large timestep.

As Eq. (5.4) indicates a direct relationship of the timestep to the minimum grid-spacing, this equation dictates the useful range of GLL nodes per element-edge. As discussed above and depicted in Fig. 2, increasing the order of spectral elements leads to clustering of nodes at the element edges and reduces Δx_{min}. While on the one hand higher order elements lead to a better approximation, on the other hand the length of the time increment has to be reduced (denoting more timesteps for the same period T, resulting in a higher computational cost). From a practical point of view, the elements with an approximation order of 5 to 9 seem an acceptable compromise.

6. Piezoelectric coupling

As mentioned before, an efficient coupling of piezoelectric patches is included into the spectral element framework. On the one hand these patches have local contributions to the mass, stiffness and damping properties of the structure, on the other hand the coupling of electrical and mechanical quantities due to the piezoelectric effect has to be considered. The well-known piezoelectric effect is not to be explained in detail here because the general equations can be found in many textbooks, see e.g. Ikeda (1990). Assuming isotropic piezoelectric actuators, the magnitude of the induced line forces and moments at the edges of a rectangular piezo actuator patch that is bonded onto the surface of a plate structure (actuator equation) can be expressed, following Banks *et al.* (1996), as

$$\begin{aligned} N_x^{pzt} &= N_y^{pzt} = \frac{-E_{pzt} h_{pzt}}{1-\nu_{pzt}} \frac{d_{31}}{h_{pzt}} V_{pzt} \\ M_x^{pzt} &= M_y^{pzt} = -\frac{1}{8} \frac{E_{pzt}}{1-\nu_{pzt}} \Big[4 \Big(\frac{h}{2} + h_{pzt} \Big)^2 - h^2 \Big] \frac{d_{31}}{h_{pzt}} V_{pzt} \end{aligned} \tag{6.1}$$

Here, h denotes the plate thickness, h_{pzt} is the thickness of the piezo element, d_{31} is a piezo-ceramic strain constant, E_{pzt} and ν_{pzt} are Young's modulus and the Poisson's ratio of the piezo patch, and V_{pzt} denotes the applied voltage. If

instead of rectangular patches, disc-shaped pzt-elements are used, the forces and moments act at those nodes nearest to the physical edges of the pzt-element, as it is depicted in Fig. 6. The line forces of the quadratic-shaped element (indicated in grey) are replaced by forces at those GLL nodes nearest to the radius of the round element (indicated in black). Mass, stiffness and damping contributions to the global system are also only considered for those areas physically covered by the pzt-element.

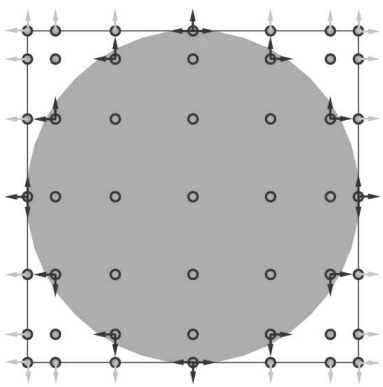

Fig. 6. Alignment of equivalent piezoelectric nodal forces (black arrows) for a pzt-disc

The sensor equation is developed for orthotropic situations in Yang and Ngoi (1999), and is used to calculate the output charge $Q(t)$

$$Q(t) = -\iint_S (F + \varepsilon_{33}^X E_3)\, dxdy + z_k \iint_S G\, dxdy \tag{6.2}$$

with

$$F(x,y) = e_{31}\frac{\partial u_0}{\partial x} + e_{32}\frac{\partial v_0}{\partial y} \qquad G(x,y) = e_{31}\frac{\partial \varphi_y}{\partial x} + e_{32}\frac{\partial \varphi_x}{\partial y} \tag{6.3}$$

The charge depends on the strain in the piezo patch, as can be seen in equation (6.3), where e_{31} and e_{32} are the coupling coefficients. For circular patches, only the proportion of the element that is physically covered by the patch is considered for the strain calculation. Because of the high density of the interior mesh, the resulting output charge is accurate even for a small wavelength corresponding to high frequency waves.

Using these equations is an efficient possibility to incorporate the electro-mechanical coupling because it avoids adding further degrees of freedom to the system, as has to be done using an approach including electrical degrees of

freedom, see e.g. Lammering and Mesecke-Rischmann (2003). It is straight forward to compute the generalised actuator forces and add them as external forces $\mathbf{F}_{ext}$ to the global system. The strains for the sensing equation (Eq. (6.2)) can be easily calculated either analytically using the strain-displacement matrix $\mathbf{B}$ or numerically from the resulting displacements. Effects of shear-lag due to the glue-layer between piezo patch and host structure can easily be implemented by loss factors, as it is done in the application shown subsequently. It is also possible to consider more refined models of the piezoelectric patches including eigenresonances and so on, but this is not in the scope of this paper and not necessary for the considered frequency range used here.

7. Application I, wave propagation in a GFRP plate

The presented methodology is used to simulate the propagation of waves in a unidirectional GFRP plate of dimensions 800 mm×800 mm that is depicted in Fig. 7. The thickness of the plate is approximately 1.5 mm, the fibre direction is in the y-direction. As can be noticed in Fig. 7, nine piezoelectric patches are attached to the structure. The piezo-discs have a diameter of 10 mm and a thickness of 0.25 mm. For the simulation, the plate is meshed with 68×68 elements using 36 nodes per element.

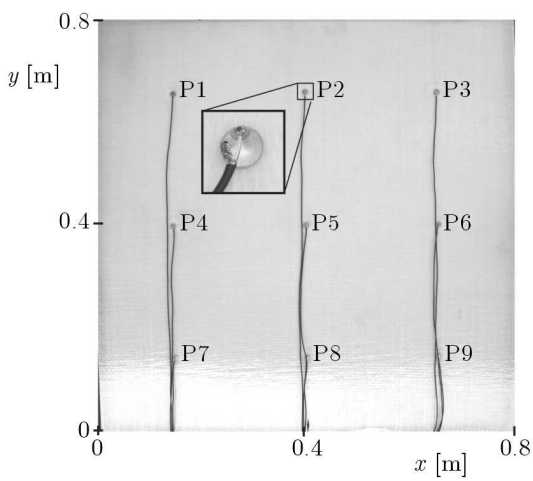

Fig. 7. GFRP plate with piezo patches

To demonstrate the capabilities of this simulation approach, the patch located in the centre (P5) is used as an actuator, and the other patches are

used as sensors. A voltage pulse signal with a carrier frequency of 100 kHz lasting for 5 cycles (windowed by an Hann-window) is used as the actuation signal, and the received sensor signals at the other patches are both measured and calculated.

In Fig. 8, the measured and simulated sensor voltage signals are compared for patches P2, P3 and P6 corresponding to 90°, 45° and 0°. For this comparison, a loss factor of 0.78 is introduced to compensate for the shear lag effect of the actuator and sensors, and Young's moduli, shear moduli and density of the plate are optimized. The signals that can be seen at the measurement voltage of P2 and P3 at the time before 0.05 ms are an electrical coupling phenomenon with the actuator channel, because the contacts are not perfectly shielded. In general, Fig. 8 shows a good agreement of the simulated and measured data including the time of flight of different wave-modes, amplitude and phase.

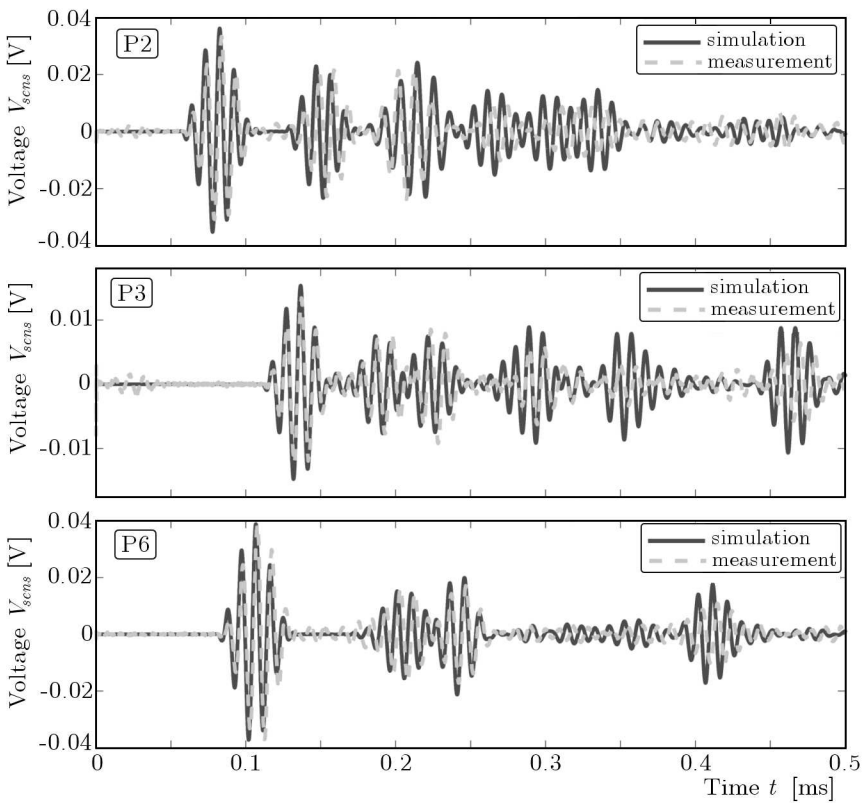

Fig. 8. Simulated and measured sensor signals for P2, P3 and P6; excitation at 100 kHz

Comparison of the signals of P2 and P6 (Fig. 8) shows the anisotropy of this plate, because both sensors have the same distance to the actuator, but the time of flight is significantly shorter to P2 that is placed in the direction of the fibres. The anisotropic characteristic becomes even more obvious by considering snapshots of the propagating waves. In Figs. 9 and 10 some of these snapshots are depicted. As the excitation signal for these plots, a windowed pulse signal with a carrier frequency of 75 kHz lasting for four cycles was used. In Fig. 9 the resulting in-plane displacement, calculated from the x- and y-displacement is depicted (in-plane waves), while in Fig. 10 the z-displacement is shown (out-of-plane waves). In Fig. 9, the same scale is used for all snapshots, because the damping of the in-plane waves is not as strong as for the out-of-plane waves, where different scales had to be used (see Fig. 10). In both figures small disturbances of the wave field can be noticed, when the travelling waves reach the piezo sensors (Fig. 9c,d and Fig. 10b,c).

In contrast to isotropic plates, where the SH_0 mode is usually not excited by bonded piezo actuators, in Fig. 9 two different wave modes, namely S_0 and SH_0 can be clearly identified, because besides the S_0 wave, there is another group of waves with a lower wave speed and wavelength. The SH_0 wave propagates predominantly in a direction close to $\pm 45°$ (see Fig. 9d,e).

In Figs. 10c and 10d, the anisotropic damping characteristics can be noticed, because travelling the wave packet in the x-direction looses its amplitude much faster than in the y-direction. Moreover, the dispersive character of the out-of plane waves is obvious, because the pulse widens with increasing runtime, in contrast to the in-plane waves that are barely dispersive.

In comparison to pure sensor data, the presented simulation methodology provides a deeper insight to many details of the wave propagation phenomena. While on a single plate the behaviour of the travelling waves is comparatively simple to predict, matters get more complicated, if more complex structures are under investigation. This makes it particularly attractive to use this simulation approach for the analysis of more complex structures.

8. Application II, wave propagation in a stringer stiffened curved panel

In the aerospace industry, typical sub-structures are curved panels with stiffeners. For that reason the presented simulation approach is demonstrated subsequently on such a panel with a radius of 2 m, which is typical for medium-sized aircraft. The geometry of the panel with its element-mesh is shown in

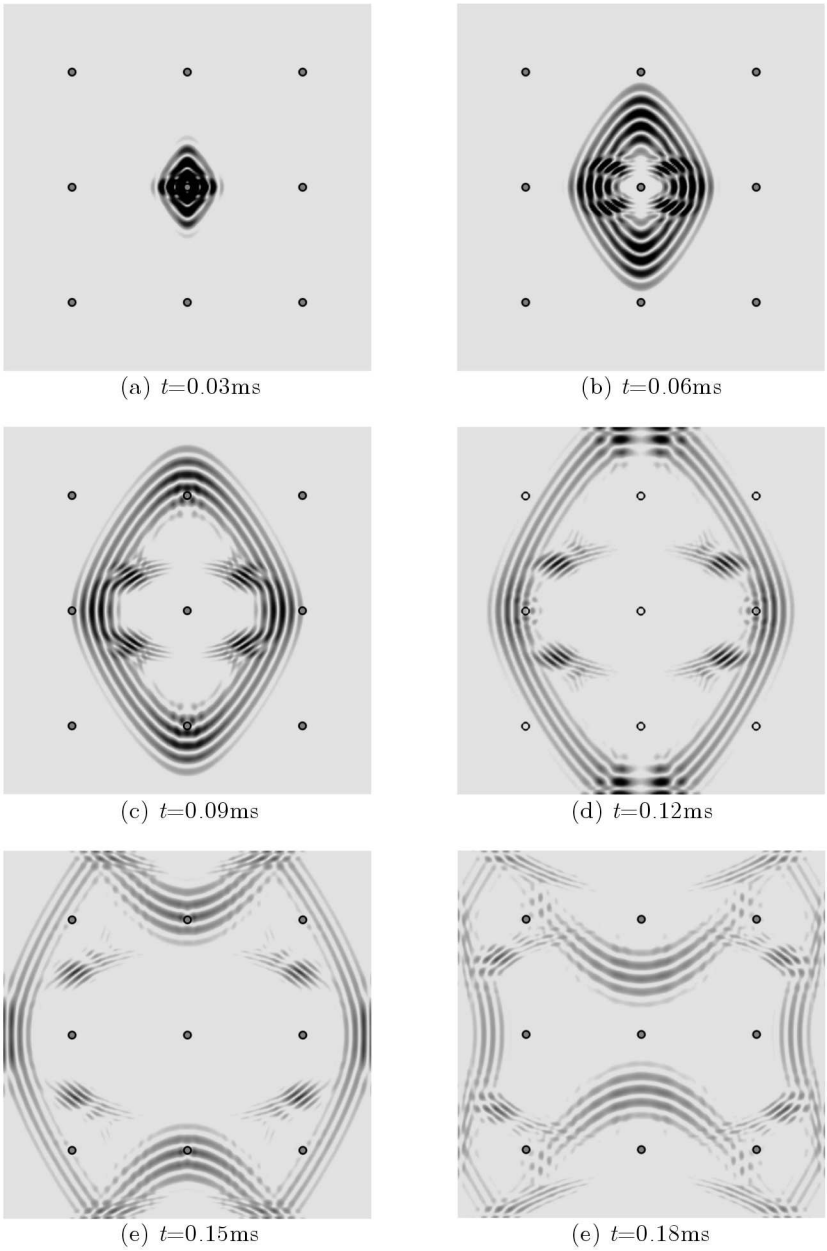

(a) t=0.03ms (b) t=0.06ms

(c) t=0.09ms (d) t=0.12ms

(e) t=0.15ms (e) t=0.18ms

Fig. 9. Snapshots of propagating in-plane-waves at 75 kHz in the GFPR plate; S_0 and SH_0 wave can be identified

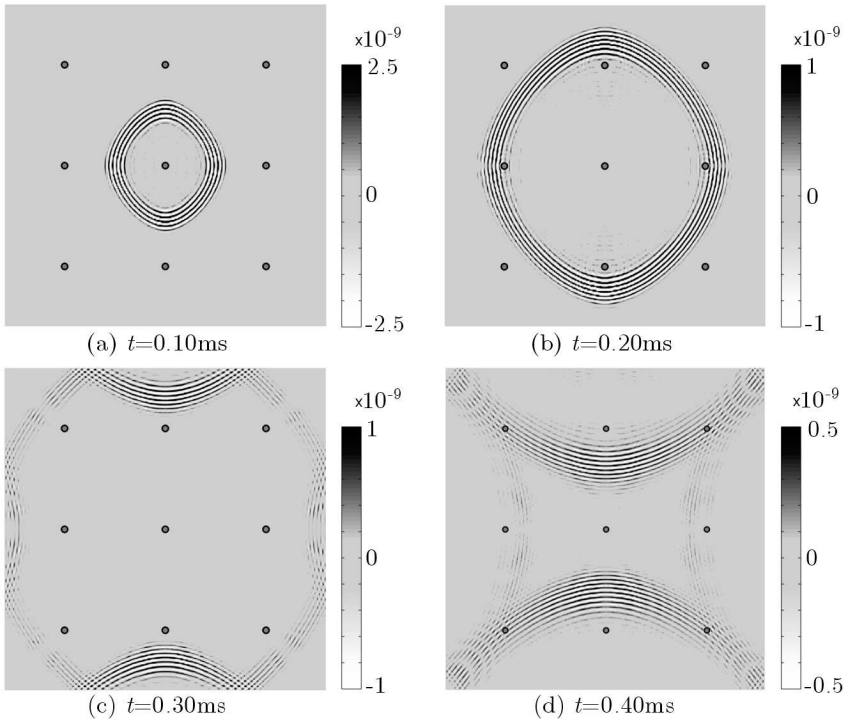

Fig. 10. Snapshots of propagating out-of-plane-waves at 75 kHz in the GFPR plate

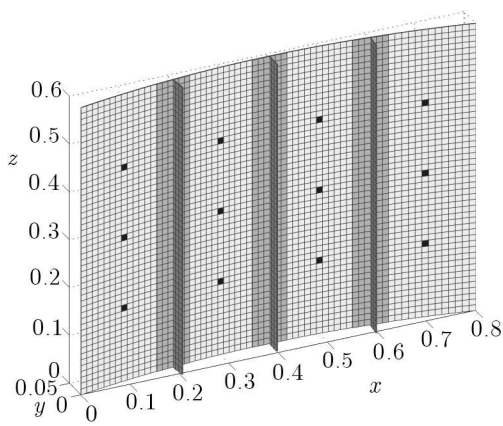

Fig. 11. Curved panel with stiffeners and piezo patches

Fig. 11, where piezo elements are indicated in black. The excitation signal is a windowed pulse signal with a carrier frequency of 50 kHz lasting for three cycles.

The T-shape stiffeners are modelled close to reality as it can bee seen in Fig. 12. For this model, an isotropic aluminium material is assumed. The connection of the base-shell to the stiffener is modelled using a five times higher attenuation factor to account for higher damping because of gluing.

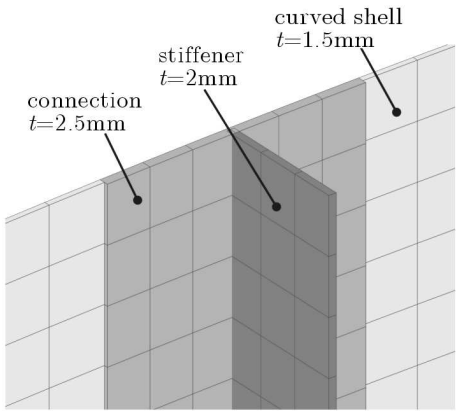

Fig. 12. Detailed view of the stiffener geometry

The subsequent figures show snapshots of different waves travelling within the panel at different time instances. The out-of-plane waves excited by the piezopatch mainly remain in the area between the two neighbouring stiffeners (see Figs. 13 to 15).

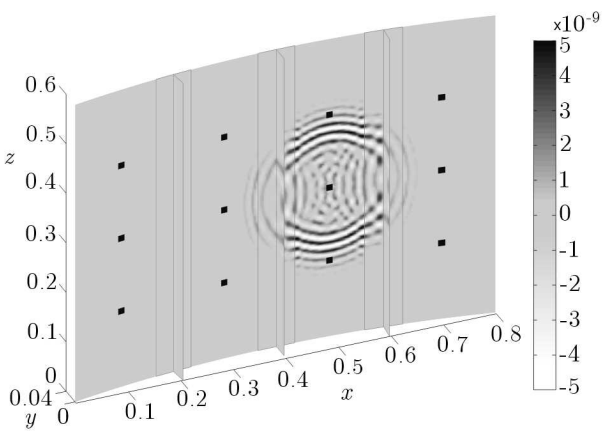

Fig. 13. y-displacement at $t = 0.10\,\mathrm{ms}$

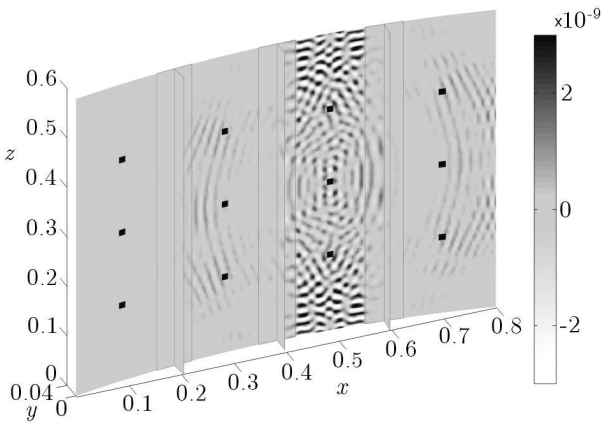

Fig. 14. y-displacement at $t = 0.20\,\mathrm{ms}$

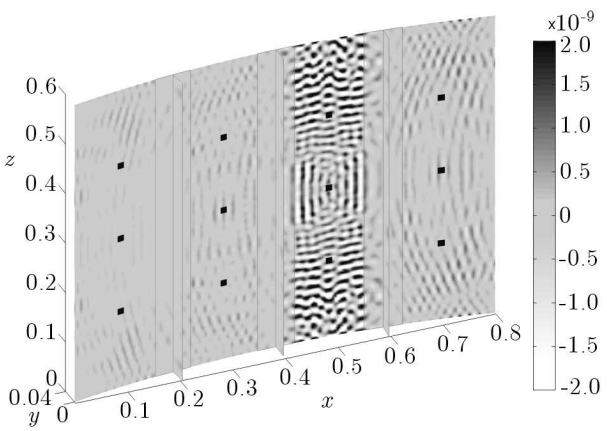

Fig. 15. y-displacement at $t = 0.30\,\mathrm{ms}$

The in-plane waves can leave this area much easier, as can be seen in Figs. 16 and 17, where the resulting in plane displacement is depicted. The in-plane waves within the base-shell excites out-of plane waves in the stiffeners, as can be seen in Fig. 17 from the shorter wavelength in the stiffeners.

As in Fig. 17 some contributions of waves with a shorter wavelength also in the base-shell are noticeable, in Fig. 18 the local in-plane displacements at the same time instance are plotted for comparison. This makes clear that those contributions arise just from the curvature of the base-shell, because the global xz-displacement contains parts from the out-of-plane wave as well.

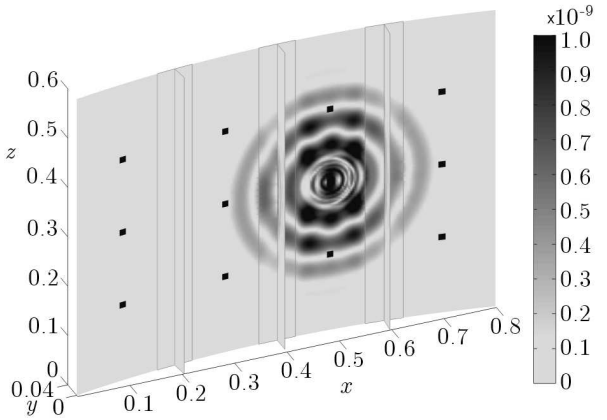

Fig. 16. xz-displacement at $t = 0.10\,\mathrm{ms}$

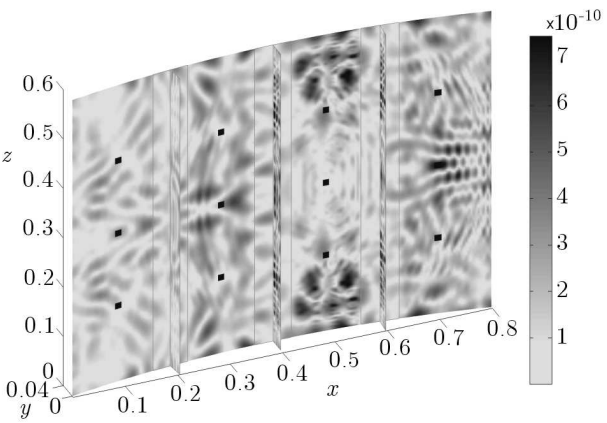

Fig. 17. xz-displacement at $t = 0.30\,\mathrm{ms}$

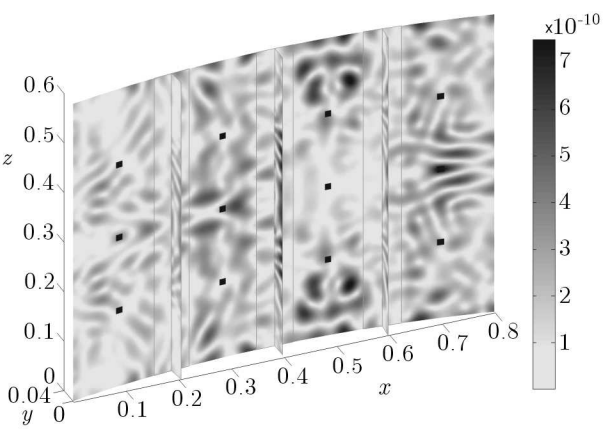

Fig. 18. Local in-plane displacement at $t = 0.30\mathrm{ms}$

9. Conclusions

The formulation of flat spectral shell elements has been presented in detail. The novelty of this contribution is, in particular, the capability of the presented formulation to include direction dependent attenuation within the spectral element framework. The construction of the damping matrix and the efficient implementation within the central difference scheme for the time integration were discussed. Moreover, piezoelectric coupling is implemented within the spectral element framework. This is done using analytical equations and avoiding additional degrees of freedom. The ability to handle damping phenomena broadens the scope of application of this methodology towards realistic simulation models especially regarding composite materials.

The proposed approach is demonstrated by two examples including a comparison to experimental data for a unidirectional GFRP plate. Simulated and measured sensor data show a good correlation and affirm the necessity to consider the attenuation. The second, pure numerical example demonstrates the application to a stiffened curved panel, a more complex structure that is often used as sub-structure in the aircraft industry.

The simulation can support a deeper understanding of the propagation behaviour of different wave modes including direction-depending attenuation, reflections from various obstacles as the stiffeners, and some more.

In the next step, the presented approach can be used to optimize actuator/sensor networks on structures including extensive parameter studies. This process can help to shorten time, cost and material consumption of pretests and may help to bring SHM a small step further to real life application and higher TRL levels.

References

1. Bagley R.L., Torvik P.J., 1985, Fractional calculus in the transient analysis of viscoelastically damped structures, *AIAA Journal*, **23**, 6, 918-925

2. Balageas D., Fritzen C.-P., Güemes A. (eds.), 2006, *Structural Health Monitoring*, Hermes Science Publishing, London UK

3. Banks H.T., Smith R.C., Wang Y., 1996, *Smart Material Structures, Modelling, Estimation and Control*, Wiley, Masson, Paris

4. BATHE K.-J., 1986, *Finite-Element-Methoden*, Springer, Berlin, Heidelberg, New York

5. BESKOS D.E., 1997, Boundary element methods in dynamic analysis: Part II (1986-1996), *App. Mech. Rev.*, **50**, 3, 149-198

6. CHO Y., ROSE J.L., 1996, A boundary element solution for mode conversion study of the edge reflections of Lamb waves, *J. Acoust. Soc. Am.*, **99**, 2079-2109

7. DAUKSHER W., EMERY A.F., 2000, The solution of elastostatic and elastodynamic problems with Chebyshev spectral finite elements, *Comput. Methods Appl. Mech. Engrg.*, **188**, 217-233

8. DELSANTO P.P., SCHECHTER R.S., MIGNOGNA R.B., 1997, Connection machine simulation of ultrasonic wave propagation in materials III: The three-dimensional case, *Wave Motion*, **26**, 329-339

9. DOYLE J.F., 1997, *Wave Propagation in Structures*, Springer, Berlin

10. FORNBERG B., 1987, The pseudospectral method; Comparisons with finite differences for the elastic wave equations, *Geophys.*, **52**, 483-501

11. GIURGIUTIU V., 2007, *Structural Health Monitoring with Piezoelectric Wafer Active Sensors*, Academic Press, Elsevier, San Diego

12. GRAVES R.W., 1996, Simulating seismic wave propagation in 3D elastic media using staggered-grid finite differences, *Bull. Seismol. Soc. Am.*, **86**, 4, 1091-1106

13. HUGHES T.J.R., 1987, *The Finite Element Method: Linear Static and Dynamic Finite Element Analysis*, Prentice-Hall Englewood Cliffs, NJ

14. IKEDA T., 1990, *Fundamentals of Piezoelectricity*, Oxford University Press, New York

15. KOMATITSCH D., MARTIN R., TROMP J., TAYLOR M.A., WINGATE B.A., 2001, Wave propagation in 2-D elastic media using a spectral element method with triangles and quadrangles, *J. Comp. Acoust.*, **9**, 2, 703-718

16. KU H., HIRSH R., TAYLOR T., 1987, A pseudospectral method for solution of the three-dimensional incompressible Navier-Stokes equations, *J. Comput. Phys.*

17. KUDELA P., OSTACHOWICZ W., 2009, A multilayer delaminated composite beam and plate elements: reflections of Lamb waves at delamination, *Mechanics of Advanced Materials and Structures*, **16**, 3, 174-187

18. KUDELA P., ZAK A., KRAWCZUK M., OSTACHOWICZ W., 2007, Modelling of wave propagation in composite plates using the time domain spectral element method, *J. Sound and Vib.*, **302**, 728-745

19. LAMMERING R., MESECKE-RISCHMANN S., 2003, Multi-field variational formulations and related finite elements for piezoelectric shells, *Smart Mater. Struct.*, **12**, 904-913

20. MANKINS J.C., 1995, Technology readiness levels, *White Paper*, **6**

21. MOSER F., JACOBS L.J., QU J., 1999, Modeling elastic wave propagation in waveguides with the finite element method, *NDT&E International*, **32**, 225-234

22. OSTACHOWICZ W., 2008, Damage detection of structures using spectral finite element method, *Computers and Structures*, **86**, 3/5, 454-462

23. OSTACHOWICZ W., KUDELA P., 2010, Wave propagation numerical models in damage detection based on the time domain spectral element method, *IOP Conf. Series: Materials Science and Engineering*, **10**, 012068

24. PATERA A.T., 1984, A spectral element method for fluid dynamics: Laminar flow in a channel expansion, *J. Comput. Phys.*, **54**, 468-488

25. PENG H., MENG G., LI F., 2009, Modelling of wave propagation in plate structures using three-dimensional spectral element method for damage detection, *Journal of Sound and Vibration*, **320**, 942-954

26. POZRIKIDIS C., 2005, *Introduction to Finite and Spectral Element Methods using Matlab*, Chapman & Hall/CRC, Boca Raton

27. RUCKA M., 2010, Experimental and numerical study on damage detection in an L-joint using guided wave propagation, *Journal of Sound and Vibration*, **329**, 1760-1779

28. SERIANI G., 2004, Double-grid Chebyshev spectral elements for acoustic wave modelling, *Wave Motion*, **39**, 351-360

29. SERIANI G., PRIOLO E., 1994, Spectral element method for acoustic wave simulation in heterogeneous media, *Finite Elem. Anal. Des.*, **16**, 337-348

30. WAGNER W., 1985, Eine geometrisch nichtlineare Theorie schubelastischer Schalen mit Anwendung auf Finite-Elemente-Berechnungen von Durchschlag- und Kontakt problemen, Dissertation, Universität Hannover, Hannover

31. YANG S., NGOI B., 1999, General sensor equation and actuator equation for the theory of laminated piezoelectric plates, *Smart Mater. Struct.*, **8**, 411-415

32. YIM H., SOHN Y., 2000, Numerical simulation and visualization of elastic waves using mass-spring lattice model, *IEEE Transactions on Ultrasonics, Ferroelectrics and Frequency Control*, **47**, 549-558

33. ZIENKIEWICZ O.W., TAYLOR R.L., ZHU J.Z., 2005, *The Finite Element Method*, 6th ed., Elsevier Butterworth-Heinemann, Oxford

Symulacja propagacji fali w kompozytach tłumionych efektem sprzężenia piezoelektrycznego

Streszczenie

W pracy przedstawiono efektywną i dokładną procedurę symulacji układów z systemem monitorowania stanu (SHM) stosowaną na wstępnym etapie projektowania takich układów i pozwalającą na redukcję czasu i kosztów niezbędnych analiz wstępnych. Procedurę oparto na metodzie elementów spektralnych w dziedzinie czasu, co umożliwiło uzyskanie optymalnie określonych macierzy bezwładności i przez to zdecydowane skrócenie czasu całkowania. Przybliżono podstawy teoretyczne metody i opisano elementy spektralne dla płaskich powłok. Przedyskutowano nową metodologię badań symulacyjnych pozwalających na wprowadzenie tłumienia anizotropowego oraz efektu sprzężenia piezoelektrycznego w ujęciu elementów spektralnych. Na kilku przykładach zaprezentowano dokładność obliczeń numerycznych poprzez porównanie ich z wynikami eksperymentu oraz wykazano ich przydatność do analizy bardziej złożonych układów, jak np. zakrzywionych paneli z lokalnymi usztywnieniami.

Manuscript received March 23, 2011; accepted for print April 19, 2011